Determination of the affinity of biomimetic peptides for uranium through the simultaneous coupling of HILIC to ESI-MS and ICP-MS

Lana Abou Zeid, Albert Pell, Marta Garcia Cortes, Hélène Isnard, Pascale Delangle, Carole Bresson

Determination of the affinity of biomimetic peptides for uranium through the simultaneous coupling of HILIC to ESI-MS and ICP-MS

Lana ABOU-ZEID[a, c, #], Albert PELL[a], Marta GARCIA CORTES[a], Hélène ISNARD [a], Pascale DELANGLE[b] and Carole BRESSON[a*]

[a] Université Paris-Saclay, CEA, Service d'Etudes Analytiques et de Réactivité des Surfaces F-91191, Gif-sur-Yvette, France

[b] Univ. Grenoble Alpes, CEA, CNRS, GRE-INP, IRIG, SyMMES, 38 000 Grenoble, France

[c] Sorbonne Université, UPMC, F-75005 Paris, France

Current address: Department of Analytical Chemistry, Ghent University, Krijgslaan 281-S12, 9000 Ghent, Belgium

* CORRESPONDING AUTHOR: Carole BRESSON

Email address: carole.bresson@cea.fr

KEYWORDS: Uranyl, multi-phosphorylated peptides, simultaneous coupling, HILIC, ESI-MS, ICP-MS, affinity scale

Abstract

Several proteins have been identified in the past decades as targets of uranyl (UO_2^{2+}) *in vivo*. However, the molecular interactions responsible for this affinity are still poorly known which requires the identification of the UO_2^{2+} coordination sites in these proteins. Biomimetic peptides are efficient chemical tools to characterize these sites. In this work, we developed a dedicated analytical method to determine the affinity of biomimetic, synthetic, multi-phosphorylated peptides for UO_2^{2+} and evaluate the effect of several structural parameters of these peptides on this affinity at physiological pH. The analytical strategy was based on the implementation of the simultaneous coupling of hydrophilic interaction chromatography (HILIC) with electrospray ionization mass spectrometry (ESI-MS) and inductively coupled plasma mass spectrometry (ICP-MS). An essential step had been devoted to the definition of the best separation conditions of UO_2^{2+} complexes formed with di-phosphorylated peptide isomers and also with peptides of different structure and degrees of phosphorylation. We performed the first separations of several sets of UO_2^{2+} complexes by HILIC ever reported in the literature. A dedicated method had then been developed for identifying the separated peptide complexes online by ESI-MS and simultaneously quantifying them by ICP-MS, based on uranium quantification using external calibration. Thus, the affinity of the peptides for UO_2^{2+} was determined and made it possible to demonstrate that (i) the increasing number of phosphorylated residues (pSer) promotes the affinity of the peptides for UO_2^{2+}, (ii) the position of the pSer in the peptide backbone has very low impact on this affinity (iii) and finally the cyclic structure of the peptide favors the UO_2^{2+} complexation in comparison with the linear structure. These results are in agreement with those previously obtained by spectroscopic techniques, which allowed to validate the method. Through this approach, we obtained essential information to better understand the mechanisms of toxicity of UO_2^{2+} at the molecular level and to further develop selective decorporating agents by chelation.

Introduction

The occurrence of uranium (U) in the environment is due to natural and anthropogenic sources [1]. Being part of the actinide family, U has no biological function and exhibits chemical and radiological toxicity, depending on its isotopic composition. Natural U (U_{nat}) displays mainly chemical toxicity driven by the interactions of the uranyl cation (UO_2^{2+}) with target biomolecules *in vivo* [2]. However, the mechanisms of toxicity of UO_2^{2+} at the cellular and molecular level are still poorly understood. The full identification of biomolecules binding specifically UO_2^{2+} *in vivo* and *in vitro* and the characterization of their interactions are essential to better describe these mechanisms and to further develop selective decorporating agents. Although few target proteins of UO_2^{2+} have been identified *in vivo* [3,4], the coordination sites responsible for their strong affinity for UO_2^{2+} are still not known. In this context biomimetic approaches, based on the synthesis of model peptides designed specifically to mimic the coordination sites of UO_2^{2+} in proteins, are very useful to determine the key parameters governing this affinity [5]. Recently, multi-phosphorylated cyclopeptides have been synthetized as models of UO_2^{2+} coordination sites in osteopontin (OPN) (Fig.1), a hyperphosphorylated target protein of UO_2^{2+} [4,6]. Such biomimetic peptides need to be validated to be representative of the suggested UO_2^{2+} coordination sites. In this purpose, studies have been devoted to the characterization of UO_2^{2+} interactions with these peptides and the determination of the associated stability constants using spectroscopic techniques such as fluorescence spectroscopy, Extended X-ray absorption fine structure (EXAFS), circular dichroism (CD) and also electrospray ionization mass spectrometry (ESI-MS) [6–10]. Through these studies, the affinity of these peptides for UO_2^{2+} was shown to increase with the number of phosphoserine residues (pSer) in their scaffold, to reach the highest value for tetra-phosphorylated peptide (pS1368), being close to the affinity constant of UO_2(OPN) [6].

The aim of this work was to develop a dedicated analytical method to determine in a single step an affinity scale of multi-phosphorylated biomimetic peptides for UO_2^{2+}. The strategy was based on the setting up of the simultaneous coupling of hydrophilic interaction liquid chromatography (HILIC) to electrospray ionization mass spectrometry (ESI-MS) and inductively coupled plasma mass spectrometry (ICP-MS) [11,12]. The UO_2(peptide) complexes could then be separated, online identified by ESI-MS

and quantified by ICP-MS in a simultaneous manner. Hence, the quantitative distribution of UO_2^{2+} within the different complexes could be determined in one single step, leading to the further determination of an affinity scale. Through this approach, complementary data to those obtained by spectroscopic techniques could be acquired in combination with the reduction of analysis time and sample consumption, which is a major advantage when only small amount of the peptides can be synthesized. A major challenge was to achieve the chromatographic separation of the UO_2^{2+} complexes while preserving the integrity of their structure, knowing that their labile character and their electrostatic interactions can lead to their dissociation during the separation processes [13]. The separation mode of HILIC seemed promising to meet this challenge since it is dedicated to the separation of polar, hydrophilic, neutral or charged compounds and is described as being suitable for the separation of metal complexes, even the labile ones [14]. To our knowledge, the separation of UO_2^{2+} complexes by HILIC has never been reported in the literature.

The first part of this work was devoted to the definition of HILIC separation conditions of several model systems containing (i) UO_2^{2+} with di- and tetra-phosphorylated peptides, pS16 and pS1368, in order to determine the effect of the number of pSer residues on UO_2^{2+} affinity (ii) UO_2^{2+} and di-phosphorylated peptide isomers, pS16 and pS18, in order to evaluate the impact of the position of pSer residues on UO_2^{2+} affinity, (iii) UO_2^{2+} in presence of cyclic pS1368 and linear linS1368 tetra-phosphorylated peptides, in order to evaluate the impact of the peptide structure on its affinity for UO_2^{2+}. Then a quantification method of UO_2^{2+} based on external calibration was developed to determine online the distribution of UO_2^{2+} within the separated complexes. Such a dedicated method allowed to measure in a single step the affinity of biomimetic peptides towards UO_2^{2+} when they are in competing complexation reaction and to determine the effect of the structural parameters of the peptides on their affinity.

1. Experimental part

1.1.Chemicals

Acetonitrile (ACN, CH_3CN, LC-MS grade) and ammonia NH_3 (20-22%) were purchased from VWR prolabo (Briare le canal, France). Ammonium acetate ($NH_4CH_3CO_2$) and toluene ($C_6H_5CH_3$, purity > 99.7 %) were supplied by Sigma Aldrich (Saint Quentin Fallavier, France). Ultrapure water (18.2 MΩ cm at 25°C) was obtained from Milli-Q purification system (Merck millipore, Guyancourt, France). Uranium (U) and bismuth (Bi) standard solutions (1000 µg mL^{-1}) in HNO_3 2% *w/w*, were provided by the SPEX Certiprep Group (Longjumeau, France). L-Tryptophan (Trp) (99% purity) was purchased from Acros Organics. Nitric acid solutions (HNO_3 2%) were prepared by diluting in ultrapure water, HNO_3 65% (Merck, France) which was distilled with evapoclean from Analab (France).

1.2. Preparation of stock solutions and samples

1.2.1. Uranium and peptide stock solutions

The uranium stock solution was prepared by diluting in ultrapure water an in-house U_{nat} solution [15] prepared in 0.5 mol L^{-1} ultrapure HNO_3 (SCP Science), to achieve a U_{nat} concentration of 10,000 µg mL^{-1} (5×10^{-2} mol L^{-1}). The U_{nat} concentration of the stock solution was determined by ICP-MS based on external calibration using U_{nat} standard solutions in HNO_3 2% and was 9,447.2 µg mL^{-1} (3.97×10^{-2} mol L^{-1}).

Di-phosphorylated peptide isomers pS16 and pS18 were synthetized, characterized and supplied by the CIBEST team at SyMMES (Univ. Grenoble Alpes, CEA, CNRS, IRIG, 38 000 Grenoble - France) following the procedures described elsewhere [8]. Linear and cyclic tetra-phosphorylated peptides pS1368 and linS1368, were supplied by Cambridge peptides (Cambridge, UK) following the procedure developed by the CIBEST team [6]. The peptide stock solutions were prepared by dissolving the adequate amount of the targeted peptide powder in 20 mmol L^{-1} $NH_4CH_3CO_2$ (pH ~ 7.4) to reach a concentration between 2 and 4 mmol L^{-1}. The concentration of the peptides was determined by external calibration, using HILIC coupled to UV/VIS in series with ESI-MS, by quantifying the Tryptophan (Trp) contained in the sequence of all peptides (UV absorption at λ = 280 nm). Trp standard solutions were obtained by diluting a Trp solution prepared at 10^{-2} mol L^{-1} in 20 mmol L^{-1} $NH_4CH_3CO_2$, in 70/30

ACN/H_2O containing 20 mmol L^{-1} $NH_4CH_3CO_2$ to reach concentrations that ranged between 5 $x10^{-6}$ mol L^{-1} and 2 x 10^{-4} mol L^{-1}.

1.2.2. Preparation of the samples

In a first step, UO_2(peptide) contact solutions were prepared by adding a very small volume (around 1.5 µL) of U_{nat} stock solution in 125-250 µL of peptide stock solution, to obtain UO_2^{2+} concentration ranging between 2 and 5 x 10^{-4} mol L^{-1} and the desired UO_2^{2+}/peptide ratio. The pH was adjusted to 7.4 using ammonia (20-22%). All solutions were systematically prepared the day before the analysis. Finally, the working samples were freshly prepared before analysis by diluting the UO_2(peptide) contact solutions by a factor of 2 or 5 in the adequate mobile phase, to reach a final UO_2^{2+} concentration of 10^{-4} mol L^{-1}, which was quantified by ICP-MS as described in section 1.4.1. The concentration of the peptides in the contact solution was determined by weight while taking into account the concentration of the peptide stock solution.

1.3.Instrumentation

1.3.1. Hydrophilic interaction liquid chromatography

An ultimate 3000 UHPLC$^+$ Dionex/Thermofisher scientific (Courtaboeuf, France), made of a degasser, a dual RS pump, an RS autosampler, a column compartment and an RS diode array detector, was used. The separation of the different sets of UO_2(peptide) complexes was carried out using Acquity BEH Amide (100 x 2.1; 1,7 µm, Waters), YMC Triart Diol (100 x 2; 1.9 µm, YMC) and Acquity BEH HILIC (100 x 2.1; 1,7 µm, Waters) columns. The composition of the desired mobile phases was obtained by online mixing in the adequate proportions, solvent A (60/40 ACN/H_2O *v/v* containing 20 mmol L^{-1} $NH_4CH_3CO_2$) and solvent B (80/20 ACN/H_2O *v/v* containing 20 mmol L^{-1} $NH_4CH_3CO_2$).

For the quantification of pS16, pS18 and pS1368 stock solutions, an YMC Triart diol (100 x 2 mm; 1,9 µm) column was used with a mobile phase composed of 70/30 ACN/H_2O *v/v* and 20 mmol L^{-1} $NH_4CH_3CO_2$. For the quantification of linS1368, an Acquity BEH HILIC (100 x 2,1; 1,7µm) column was used and the mobile phase was made of 68/32 ACN/H_2O *v/v* and 20 mmol L^{-1} $NH_4CH_3CO_2$. In all the cases, the separation was run in isocratic mode at a flow rate of 300 µL min^{-1} and the injection volume was 3 µL.

The retention factor *k* of the analytes were calculated following the equation (1):

$$k = \frac{(t_R - t_0)}{t_0} \text{ (Equation 1)}$$

Where t_R is the retention time (min) of the analyte, determined by HILIC-ESI-MS, t_0 is the void time of unretained marker, toluene (10^{-4} mol L^{-1}, V_{inj} = 1 µL), determined by HILIC-UV/VIS at λ = 254 nm.

The selectivity and resolution factors of the separations, α and R_s respectively, were calculated based on the equations 2 and 3:

$$\alpha = \frac{k_2}{k_1} \text{ (Equation 2)}$$

$$R_s = 1.18 \text{ x } \frac{t_{R2} - t_{R1}}{W_{0.5h1} + W_{0.5h2}} \text{ (Equation 3)}$$

With analyte 2 more retained than analyte 1. $W_{0.5}$ corresponds to full width half-maximum of each peak.

1.3.2. Mass spectrometers

The ESI mass spectrometer was a triple quadrupole TSQ Quantum Ultra™ (Thermo Fisher scientific, San Diego CA, USA) equipped with an H-ESI II ionization probe. All mass spectra were recorded in negative ionization mode with the following parameters: spray voltage -3.5 kV, temperature of the probe 120°C and temperature of the capillary transfer 360°C. In all cases and in agreement with previous studies [6,8], double charged $[UO_2(peptide)]^{2-}$ complexes with 1:1 stoechiometry were observed. For the sake of clarity, the UO_2^{2+} complexes were denoted along the manuscript UO_2(peptide), by omitting the charge. Mass spectra were acquired in full scan mode (*m/z* 400-1500) and in single ion monitoring (SIM) mode, by selecting the *m/z* ratio associated to the targeted free peptides and UO_2(peptide) complexes (spectral width: ± 0.5 *m/z*).

The ICP-MS instrument was a single quadrupole XSeriesII (Thermo Fisher Scientific). The sample introduction system consisted of a perfluoroalkoxy PFA-ST nebulizer operating at 200 µL min^{-1} followed by a quartz cyclonic spray chamber thermostated at 3 °C (PC3 system, ESI). The simultaneous coupling of HILIC to ESI-MS and ICP-MS was performed according to the setting up described in our previous work [11] and presented in Fig.2. In order to prevent any carbon deposition due to the use of organic solvents, additional 8 mL min^{-1} oxygen flow rate was introduced in the plasma, through an "additional gas port" located in the spray chamber [16,17]. A platinum skimmer, a sampler cone and a

1 mm inner diameter injector were additionally used for this purpose. The parameters were checked daily using a 25 ng mL^{-1} U_{nat} standard solution introduced in the ICP-MS at 6.7 µL min^{-1} along with a 10 ng mL^{-1} Bi in HNO_3 2% at 140 µL min^{-1} (Fig.2). The chromatograms were recorded based on the signal of ^{238}U and ^{209}Bi with an integration time of 90 ms for each isotope.

1.4.Online quantification of the UO_2(peptide) complexes

Samples were analyzed using the simultaneous coupling of HILIC to ESI-MS and ICP-MS. The separated UO_2(peptide) complexes were online identified by ESI-MS and simultaneously quantified by ICP-MS. For this purpose, external calibration was selected as quantification method for the determination of total UO_2^{2+} concentration in the samples, denoted $[UO_2^{2+}]_{total}$, since the uncertainty range (5-15%) provided by this method is adequate for our study.

1.4.1. Determination of the total UO_2^{2+} concentration in the working samples

Calibration was performed by introducing U_{nat} standard solutions into the ICP-MS under flow injection analysis mode (FIA), employing the same mobile phase composition and flow rate as used when coupling to the separation. In non-complexing medium, hydrolysis dominates the speciation of UO_2^{2+}, potentially leading to its precipitation depending on its concentration [18]. Therefore, the tetra-phosphorylated peptide pS1368 was added to the U_{nat} standard solutions in an equimolar ratio to prevent this phenomenon, but also to yield specific standard solutions of UO_2(peptide) complexes. Five levels of calibration were considered with U_{nat} concentration ranging from 8 to 40 µg mL^{-1}. The calibration curve was established daily by plotting the mean value of the peak areas as a function of U_{nat} concentrations; each standard being injected in triplicate. The repeatability of the measurements, determined from the RSD of the peak areas for each concentration, was between 1% and 4% (< 15%).

1.4.2. Quantification of UO_2^{2+} in the separated UO_2(peptide) complexes

This step was performed by integrating the total area of the chromatographic peak of each UO_2(peptide) complex and by further determining the corresponding concentration using the calibration curve. During the separation, adsorption of free or weakly complexed UO_2^{2+}, on the stationary phase can occur. To recover UO_2^{2+} adsorbed on the column, successive injections of the tetra-phosphorylated peptide pS1368 were carried out after each chromatographic run until the background of ^{238}U signal was less than 10^3

cps. The concentration of this fraction of UO_2^{2+}, denoted $[UO_2^{2+}]_{free}$, was then determined based on external calibration, by summing the area of the peaks resulting from the injections of pS1368. A cleaning process was further carried out to eliminate any adsorbed peptide residues, using 5/95 ACN/H_2O *v/v* containing 20 mmol L^{-1} CH_3COOH, followed by the column regeneration with the working mobile phase working.

The quantitative distribution of UO_2^{2+} among the eluted species, expressed in percent (%), was determined according to the Equation 4.

$$\% \, UO_2^{2+}{}_X = \frac{[UO_2^{2+}]_X}{[UO_2^{2+}]_{total}} \quad \text{(Equation 4)}$$

With X being free UO_2^{2+} or UO_2(peptide) complexes.

The mass balance was expressed as the ratio of the sum of the concentrations of UO_2^{2+} in its free and complexed forms, to the total concentration of UO_2^{2+} in the sample, according to Equation 5.

$$\text{Mass balance (\%)} = \frac{\sum [UO_2^{2+}]_{UO2(peptide1)} + [UO_2^{2+}]_{UO2(peptide2)} + [UO_2^{2+}]_{Free}}{[UO_2^{2+}]_{total}} \quad \text{(Equation 5)}$$

During the HILIC-ICP-MS coupling and the FIA mode, the stability of the ^{238}U signal was monitored using bismuth (^{209}Bi) as internal standard, added at 10 ng mL^{-1} in the nitric acid makeup solution (Fig.). The stability of the ^{209}Bi signal during an acquisition cycle was checked by calculating the relative standard deviation RSD (%) of measurements acquired continuously. The RSD was 1.9%, which reflects good stability of the signal during an acquisition cycle (< 15%). The stability of the ICP-MS response was also daily checked by calculating the standard deviation of the averaged ^{209}Bi measurements for all acquisitions cycles. As for example, for a maximum of 11 acquisition cycles, an RSD between 1 and 5.9% was obtained, which is acceptable for our applications.

2. Results and discussion

2.1. Definition of the HILIC conditions for separating UO_2(peptide) complexes

The achievement of the HILIC separation of the UO_2(peptide) complexes is a crucial step to be able to develop our method. Due to the particularity of UO_2^{2+} complexes, few chromatographic techniques are suitable to perform such challenging separations [13]. The ones encountered in the literature are mainly size exclusion chromatography (SEC) [3,19–23] and immobilized metal affinity chromatography (IMAC) [24], to investigate the interactions of UO_2^{2+} with proteins. Furthermore, the limitation of these separation techniques lies in their low separation resolution and in some cases their incompatibility to ESI-MS coupling. The preservation of UO_2^{2+} complexes during elution is of great concern since dissociation is often observed for such labile species during the chromatographic process. Even though the UO_2(peptide) complexes are known to be fully formed in the samples as indicated by their stability constants measured at pH 7.4 [6,10], they may fully or partially dissociate on the column. One way to limit this dissociation is to use an excess of the peptides in the samples. However, full dissociation was observed for complexes containing cyclic peptides with no or only one pSer in their sequence, whatever the column and the UO_2^{2+}:peptide proportion (data not shown). By contrast, UO_2^{2+} complexes with multi-phosphorylated peptides and having stability constants higher or equal to 10^{10}, could be detected using an excess of di- and tetra-phosphorylated peptides, from 2 to 10 equivalents. It must be mentioned that several UO_2^{2+}:peptide proportions were tested, but only the chromatograms obtained with the proportions that allowed to detect all the separated complexes, at least by ICP-MS, are presented in this part.

In our previous work, the Acquity BEH amide column with a mobile phase made of 70/30 ACN/H_2O *v/v* and 20 mmol L^{-1} $NH_4CH_3CO_2$ allowed a successful separation of the free multi-phorphorylated peptides [25]. Therefore, we first evaluated these conditions to separate the UO_2^{2+} complexes containing these peptides, but successful results were obtained only for the complexes formed with the ps16 and ps18 isomers (Fig.1). As shown in Fig.3-a, UO_2(pS16) and UO_2(pS18) complexes were separated with a good selectivity (α=1.3) and baseline resolution (Rs= 2.2). The availability of the pSer group in different positions in the peptide scaffold (Fig.1) could explain the achievement of the separation

through differential interactions of the pSer with the amide function of the stationary phase, as previously observed for the free peptides [25].

As stated above, these chromatographic conditions did not allow the separation of the UO_2(pS16)/ UO_2(pS1368) and UO_2(pS1368)/ UO_2(linS1368) sets of complexes, even by increasing the acetonitrile content of the mobile phase while keeping the salt concentration constant. A less polar stationary phase, grafted by diol functional group (YMC Triart Diol) led to the separation of UO_2(pS16) and UO_2(pS1368) with an improved selectivity ($\alpha = 2.3$) and resolution ($Rs = 3.9$), using 72% of ACN in the mobile phase (Fig.3-b). As seen in (Fig.3-b), the UO_2(pS16) complex could not be observed by ESI-MS despite the high excess of pS16 added to pS1368 and UO_2^{2+}. In the chromatogram recorded by ICP-MS, we could observe a peak of low intensity eluting at the same retention time as free pS16, which may be reasonably assigned to UO_2(pS16). The peak eluting at 4 min was attributed to UO_2(pS1368), thanks to its identification by ESI-MS. Furthermore, free pS1368 was not detected by ESI-MS, allowing to suggest that this peptide, which exhibits a high affinity for UO_2^{2+}, is fully coordinated.

Acquity BEH HILIC hybrid silica column was selected to separate UO_2(pS1368) and UO_2(linS1368) containing tetra-phosphorylated peptides having the same peptide sequence but different cyclic/linear structure. A mobile phase composed of 68/32 ACN/H_2O *v/v* and 20 mmol L^{-1} $NH_4CH_3CO_2$ yielded the best separation of the two complexes with good selectivity (α=8.1) and resolution (Rs=5.6) (Fig.3-c). The UO_2^{2+} complex formed with the cyclic peptide eluted earlier than the complex containing the linear one. This allows to suggest that the accessibility of the polar groups of the stationary phase to interact with the complexes is linked to the structuration of the peptide upon its complexation to UO_2^{2+}. To our knowledge, the use of hybrid silica column has never been described in the literature to separate metal complexes. Only one study reports the use of a bare silica column to separate gadolinium-based contrast agents [26], while most of the separations of transition metal complexes such as Fe, Cu and Ni, were carried out with stationary phases grafted by zwitterionic, diol and amide functions [14,27]. In our study, dedicated HILIC conditions were set up to successfully separate a set of UO_2(peptide) complexes with good selectivity and baseline resolution. These results highlight the potential of HILIC to separate UO_2^{2+} complexes, known to be challenging. Thus, we reported the first separations of UO_2^{2+} complexes ever described in the literature, using HILIC.

2.2 Evaluation of the effect of the structure of the peptides on UO_2^{2+} affinity

2.2.1. Effect of the number of phosphorylated residues in the peptide backbone

When designing biomimetic peptides, the selection of the amino acid to build the peptide backbone is of prime importance since the functional complexing groups of these amino acids will be involved in the UO_2^{2+} coordination. Phosphorylated amino acids, mainly pSer are of major concern, knowing that UO_2^{2+} exhibits high affinity for phosphate groups [28]. Furthermore, some of UO_2^{2+} target proteins such as OPN, are highly phosphorylated and are suspected to interact with UO_2^{2+} through their pSer sites [6,29]. Therefore, the effect of phosphorylation on UO_2^{2+} affinity has gained a lot of interest and was studied by using a peptide representative of site 1 of calmodulin [30,31] and phosphorylated model peptides of a specific sequence of β-casein [32]. The phosphorylation of these model peptides induced an increase of their affinity towards UO_2^{2+} in comparison to their non-phosphorylated counterparts.

In our work, the effect of phosphorylation on UO_2^{2+} affinity was evaluated in a single step by applying the analytical approach that we developed through the simultaneous coupling of HILIC to ESI-MS and ICP-MS. Several ratios of di- and tetra-phosphorylated peptides pS16 and pS1368 were added to UO_2^{2+} at pH 7.4. Knowing that the conditional stability constant of UO_2(pS16) is lower than that of UO_2(pS1368) (Fig.1), a higher excess of pS16 was added to UO_2^{2+} in comparison to pS1368. The quantitative distribution of UO_2^{2+} among the separated peptide complexes was determined through the quantification method described in the experimental part, which allowed to assess the differential affinity of the peptides towards UO_2^{2+}. The total UO_2^{2+} concentration in each sample was firstly measured in duplicate by ICP-MS before the separation and the values are listed in Table 1, as well as targeted and experimental xUO_2^{2+}:ypS1368:zpS16 proportions.

Table 1: Total concentration of UO_2^{2+} in each sample $[UO_2^{2+}]_{total}$ measured in duplicate, relative deviation* of the values, experimental concentration of pS1368 and pS16 in the samples and experimental xUO_2^{2+}:ypS1368:zpS16 proportions. For simplification, the samples containing different x:y:z proportions were assigned by a letter (A-E).

Targeted xUO_2^{2+}:ypS 1368:zpS16	**$[UO_2^{2+}]_{total}$ µg mL^{-1} (mol L^{-1})**		**Relative deviation* (%)**	**[pS1368] mol L^{-1}**	**[pS16] mol L^{-1}**	**Experimental xUO_2^{2+}:ypS1368 :zpS16 (sample N)**
	Value 1	Value 2				
2:0:20	20.5 (8.6 x10^{-5})	20.3 (8.5 x10^{-5})	1.2	0	9.2 x10^{-4}	2:0:21.2 **(A)**
2:0.5:20	20.8 (8.7 x10^{-5})	20.9 (8.8 x10^{-5})	0.7	2.3 x10^{-5}	9.1 x10^{-4}	2:0.5:20.9 **(B)**
2:2:2	30.5 (1.3 x10^{-4})	31.4 (1.3 x10^{-4})	2.9	1.2 x10^{-4}	1.2 x10^{-4}	2:1.9:1.9 **(C)**
2:3:1	39.8 (1.7 x10^{-4})	39.7 (1.7 x10^{-4})	0.3	1.7 x10^{-4}	6.0 x10^{-5}	2:2.1:0.7 **(D)**

2:4:0	33.9 (1.4 x10^{-4})	35.5 (1.5 x10^{-4})	4.6	4.6 x10^{-4}	0.0	2:6.4:0 **(E)**

*Relative deviation (value1-value 2)/(value 1)

As can be seen in Table 1, a relative deviation ranging between 0.3 and 4.6 % shows good repeatability of the measurements.

The chromatograms simultaneously recorded by ESI-MS and ICP-MS, using the YMC Triart Diol column to separate the complexes, are presented in Fig.4. The peak of free tetra-phosphorylated peptide pS1368 was observed by ESI-MS only when it was in excess relatively to UO_2^{2+}, whereas the one of pS16 was detected for all proportions. The peak corresponding to UO_2(pS1368) was detected by ESI-MS and ICP-MS for all proportions whilst the one of UO_2(pS16) was observed exclusively by ICP-MS and only when pS16 was in large excess compared to UO_2^{2+} and pS1368, that is for samples A and B. This indicates that pS1368 seems to fully complex UO_2^{2+} when they are in equimolar proportions or less, while pS16 is weakly complexed even when it is present in large excess with respect to UO_2^{2+}. The quantitative distribution of total UO_2^{2+} among the di- and tetra-phosphorylated peptide complexes and the mass balance, expressed in percent (%) could be calculated using Equation 4 and 5, respectively and are presented in the diagram of Fig.5. In the presence of three equivalents of pS1368 (Sample E), 93% of total UO_2^{2+} was involved in UO_2(pS1368) and 5% was under free form. When the proportion of pS1368 decreased compared to that of pS16, only the fraction of free UO_2^{2+} increased to reach 42% for equimolar conditions $2UO_2^{2+}$:2pS1368:2pS16 (sample C), while 56% of total UO_2^{2+} remained involved in UO_2(pS1368). Even when pS16 was in large excess compared to pS1368 and UO_2^{2+} (Sample B), up to 91% of total UO_2^{2+} was under free form and the remaining fraction was involved in UO_2(pS1368). Since UO_2(pS16) could not be quantified, its fraction was estimated to be 0.2% by calculating the ratio of the peak areas of this complex to that of total UO_2^{2+}.

Thus, it can be concluded that the addition of three equivalents of pS1368 (Sample E) to UO_2^{2+} led to the complexation of 93% of the latter, while 10 equivalents of pS16 (Sample A) were not enough to complex less than 1% of UO_2^{2+}. When these two peptides were present in equimolar proportion with respect to UO_2^{2+}, half of the total UO_2^{2+} was complexed by pS1368 while the remaining half was under free form. This results confirms that the tetra-phosphorylated peptide exhibits a higher affinity for UO_2^{2+}

compared to the di-phosphorylated one, in agreement with the values of the conditional stability constants previously reported, which allows to validate the method [6].

2.2.2. Effect of the position of phosphorylated residues in the peptide backbone

In addition to the major role played by the number of pSer residues to complex UO_2^{2+}, the coordination ability of these residues might be affected by their position in the peptide backbone and their neighboring amino acids through steric effect [8]. In this part, the impact of the position of pSer residues on UO_2^{2+} affinity was evaluated by adding di-phosphorylated peptide isomers pS16 and pS18 in equimolar proportions to UO_2^{2+}, knowing that these two peptides exhibit the same sequence but the pSer are in different positions in the cyclic peptide scaffold (Fig.1). The formed complexes were separated using the Acquity BEH amide column, and the chromatograms obtained simultaneously by ESI-MS and ICP-MS are presented in Fig.3-a.

Since these complexes are identical in terms of structure and charge, the amount of free UO_2^{2+} potentially adsorbed on the column was considered to be also identical. Therefore, the quantitative distribution of UO_2^{2+} among the two isomeric complexes was determined by calculating the ratio of the peak areas $A(^{238}U_{UO_2(pS18)})/A(^{238}U_{UO_2(pS16)})$ from the chromatograms recorded by ICP-MS, for measurements carried out in triplicate. The average ratio was 1.30 and the RSD was 6.2%, reflecting good repeatability of the measurements. The ratio close to unity shows that UO_2^{2+} did not preferentially coordinate one of the two isomers, allowing to deduce that the position of the pSer group in the peptide backbone has very weak influence on the affinity of these peptides towards UO_2^{2+}. This result is in agreement with the conditional stability constants of the two complexes, being $\log K^{pH=7.4}$ (UO_2(pS18)) = 10.1 and $\log K^{pH=7.4}$ (UO_2(pS16)) = 10.3 [8].

2.2.3. Effect of the cyclic/linear structure of the peptide backbone

The structure of the biomimetic peptides plays a key role in the coordination of UO_2^{2+}, which is directly related to the degree of flexibility of the peptide backbone [5]. The pre-organized cyclic peptides considered in this work were designed specifically to complex UO_2^{2+} in its equatorial plane (Fig.1). Linear peptides of equivalent sequence are more flexible and must therefore adapt their conformation around UO_2^{2+} for an efficient coordination. The structure of the peptide has therefore a direct effect on

its affinity for UO_2^{2+} [7]. In this part, the method developed by HILIC-ESI-MS/ICP-MS was applied to measure online and in a single step the affinity towards UO_2^{2+}, of tetra-phosphorylated peptides with the same sequence but cyclic (pS1368) and linear (lins1368) structure. Variable proportions of the pS1368 and lins1368 were added to UO_2^{2+}, in a competitive complexation reaction.

Measured total UO_2^{2+} concentration in each sample before separation, targeted and experimental xUO_2^{2+}:ypS1368:zlinS1368 proportions are summarized in Table 2.

Table 2 : Total concentration of UO_2^{2+} in each sample $[UO_2^{2+}]_{total}$ measured in duplicate, relative deviation (%) of the values, experimental concentration of pS1368 and linS1368 in the samples and experimental xUO_2^{2+}:ypS1368:zlinS1368 proportions. For simplification, the samples containing different x:y:z proportions were assigned by a letter (A-E).

Targeted xUO_2^{2+} :ypS1368 :zlinS1368	**$[UO_2^{2+}]_{total}$ µg mL^{-1} (mol L^{-1})**		**Relative deviation (%)**	**[pS1368] mol L^{-1}**	**[linS1368] mol L^{-1}**	**Experimental xUO_2^{2+} :ypS1368 :zlinS1368 (sample N)**
	Value 1	**Value 2**				
2:4:0	28.2 (1.2 x10^{-4})	28.4 (1.2 x10^{-4})	0.7	4.5 x10^{-4}	0	2:7.5:0 **(A)**
2:3:1	27.5 (1.2 x10^{-4})	27.6 (1.2 x10^{-4})	0.3	1.9 x10^{-4}	6.1 x10^{-5}	2:3.2:1 **(B)**
2:2:2	33.9 (1.4 x10^{-4})	34.8 (1.5 x10^{-4})	2.7	1.4 x10^{-4}	1.4 x10^{-4}	2:2:1.9 **(C)**
2:0.5:3.5	24.0 (1.0 x10^{-4})	23.9 (1.0 x10^{-4})	0.6	3.7 x10^{-5}	2.4 x10^{-4}	2:0.7:4.6 **(D)**
2:0:4	28.7 (1.2 x10^{-4})	28.1 (1.2 x10^{-4})	2.1	0	5.6 x10^{-4}	2:0:9 **(E)**

As reported in Table 2, the relative deviation between the values obtained for each replicate was between 0.3 and 2.7%, showing good repeatability of the measurements. The chromatograms simultaneously recorded by ESI-MS and ICP-MS, using the Aquity BEH HILIC column to separate the complexes, are shown in Fig.6.

As shown in Fig.6, the peak of free pS1368 in the chromatograms recorded by ESI-MS was observed only when it was in excess relatively to UO_2^{2+} (samples A and B), whilst the one of linS1368 was detected for all ratios. Furthermore, the peak corresponding to UO_2(pS1368) was observed by ESI-MS and ICP-MS for all proportions whilst the one of UO_2(linS1368) was detected exclusively when linS1368 was in large excess compared to UO_2^{2+}. All these observations indicate that pS1368 is fully bound to UO_2^{2+} in equimolar proportion or less, while linS1368 is weakly engaged in the complexation even when it was added in large excess. The quantitative distribution of total UO_2^{2+} among the different complexes and the mass balance, expressed in percent (%) could be calculated using Equation 4 and 5, respectively and are presented in the diagram of Fig.7. When UO_2^{2+} was in the presence of an excess of pS1368, 97% of total UO_2^{2+} were involved in the complexation while the remaining fraction was under free form (Sample A). When the proportion of pS1368 decreased in favor of that of its linear equivalent,

the fraction of free UO_2^{2+} increased significantly, while the fraction of UO_2^{2+} engaged in UO_2(linS1368) slightly increased (Sample B-D). Finally, excess of linS1368 peptide led to the involvement of only 12% of the total UO_2^{2+} in the corresponding complex, while 77% was in the free form (Sample E).

All of these results show that UO_2^{2+} coordinates preferentially the cyclic peptide in comparison with the linear one. The cyclic structure of the peptide confers a higher stability to the UO_2^{2+} complexes than the linear structure, through the more efficient coordination conferred by the preorientation of the four phosphate groups in the equatorial plane of UO_2^{2+} [33]. Owing to our approach, we were able to determine the affinity constant of UO_2(linS1368). The conditional stability constants of UO_2(pS1368) and UO_2(linS1368) are expressed according to the equilibria shown in equations 6 and 7.

$$UO_2^{2+}{}_{free} + pS1368_{free} \leftrightarrows UO_2(pS1368), \text{ with } K_{UO_2(pS1368)} = \frac{[UO_2(pS1368)]}{[UO_2^{2+}]_{free}\,[pS1368]_{free}} \quad \text{(Equation 6)}$$

$$UO_2^{2+}{}_{free} + linS1368_{free} \leftrightarrows UO_2(linS1368), \text{ with } K_{UO_2(linS1368)} = \frac{[UO_2(linS1368)]}{[UO_2^{2+}]_{free}\,[linS1368]_{free}} \quad \text{(Equation 7)}$$

From equations 6 and 7, the logarithmic expression of $\frac{K_{UO_2(pS1368)}}{K_{UO_2(linS1368)}}$ is:

$$\log\frac{K_{UO_2(pS1368)}}{K_{UO_2(linS1368)}} = \log K_{UO_2(pS1368)} - \log K_{UO_2(linS1368)} = \log\frac{[linS1368]_{free}}{[pS1368]_{free}} \quad \text{(Equation 8)}$$

$$\log K^{pH7.4}(UO_2(linS1368) = \log K^{pH7.4}(UO_2(pS1368) - \log\frac{[linS1368]free}{[pS1368]free} \quad \text{(Equation 9)}$$

The intersection point of the distribution curves of UO_2(pS1368) and UO_2(linS1368) fractions (Fig.7) corresponds to an equal percentage of both complexes. allowing to deduce their concentration: $[UO_2(pS1368)] = [UO_2(linS1368)] = 7\%$ of $[UO_2^{2+}]_{total} = 7.11 \pm 0.12 \times 10^{-6}$ mol L^{-1}, knowing that $[UO_2^{2+}]_{total} = 10^{-4}$ mol L^{-1}.

The concentration of linS1368 was deduced from the intersection point Fig.7 and was $3.59 \pm 0.06 \times 10^{-4}$ mol L^{-1}, while that of pS1368 was estimated at $2.34 \pm 0.08 \times 10^{-5}$ mol L^{-1} by plotting the same curves, but as a function of the pS1368 concentrations. Therefore, a concentration of the linear peptide 15 times higher than that of the cyclic peptide was needed to obtain an equal distribution of UO_2^{2+} between the

linear and the cyclic peptide complexes. The total concentrations of the peptides are expressed according to equations 10 and 11:

$$[\text{linS1368}]_{\text{Total}} = [UO_2(\text{linS1368})] + [\text{linS1368}]_{\text{free}} = 3.59 \pm 0.06 \times 10^{-4} \text{ mol L}^{-1} \quad \text{(Equation 10)}$$

$$[\text{pS1368}]_{\text{Total}} = [UO_2(\text{pS1368})] + [\text{pS1368}]_{\text{free}} = 2.34 \pm 0.08 \times 10^{-5} \quad \text{(Equation 11)}$$

Taking into account the concentrations of the different species calculated above, as well as the value of $\log K^{pH7.4} UO_2(\text{pS1368}) = 11.3$ [6], the equation 8 becomes:

$$\log K^{pH7.4}(UO_2(\text{linS1368}) = 11.3 - \log(21.64 \pm 1.63) = 9.97 \pm 0.03 \quad \text{(Equation 12)}$$

The constant determined through our methodology allows to deduce that the affinity of the linear tetra-phosphorylated peptide for UO_2^{2+} is more than one order of magnitude lower than its cyclic counterpart at pH 7.4. This result confirms the impact of the peptide structure on the affinity for UO_2^{2+}, that is in agreement with the behavior also observed for proteins. For example, the structure of OPN is not defined and upon complexation with UO_2^{2+}, its secondary structure undergoes modifications to effectively position 4 pSer residues in the UO_2^{2+} equatorial plane [6]. Thus, a structure fitting the coordination of UO_2^{2+} is necessary at the scale of an entire protein as well as at the scale of a small peptide to form UO_2^{2+} complexes of high stability.

Conclusion

In this work, a dedicated analytical approach was developed to separate UO_2^{2+} complexes formed with multi-phosphorylated biomimetic peptides, to characterize, and quantify them online and in a single step. To reach this aim, we implemented the simultaneous coupling of HILIC to ESI-MS and ICP-MS. Separations of the complexes containing positional isomers, peptides with two and four pSer residues as well as cyclic and linear tetra-phosphorylated peptides of the same sequence, were successfully achieved using columns with amide, diol and hybrid silica stationary phases. We developed the first separations of UO_2^{2+} complexes by HILIC ever described in the literature for complexes with conditional stability constants of 10^{10} or higher at pH 7.4. Owing to the dedicated method that we developed, quantify we were able to determine on line the quantitative distribution of UO_2^{2+} among the separated complexes. Thus, the effect of the structure of the peptides on their affinity towards UO_2^{2+} was determined and we showed that (i) the cyclic tetra-phosphorylated peptide pS1368 has the highest

affinity for UO_2^{2+} compared to peptides with a lower degree of phosphorylation, highlighting the high affinity of UO_2^{2+} for phosphate-rich binding sites in proteins. (ii) the pSer position in the peptide sequence had no significant impact on the affinity for UO_2^{2+}, in agreement with the literature results obtained by multiple spectroscopic techniques independently for each sample (iii) the cyclic structure of the tetra-phosphorylated peptide favors the UO_2^{2+} complexation compared to its linear analogue. In addition, we determined the affinity constant of the linear tetra-phosphorylated peptide, being ($\log K^{pH7.4}(UO_2(linS1368)$ = 9.97 ± 0.03.

Overall, this work highlights the powerful simultaneous coupling of HILIC to ESIMS and ICPMS to determine in a single step the effect of several structural parameters of biomimetic peptides on their affinity towards UO_2^{2+} when they are in a competing complexation reaction. A quick and reliable determination of stability of the UO_2(peptides) complexes is of prime importance to access deeper fundamental information on UO_2^{2+} toxicity but also to be able to develop *in vivo* decorporating agents based on chelation. This approach can be extended to the evaluation of the affinity of these biomimetic peptides for other actinides (Pu, Am, Cm…). Moreover, it can be implemented for the screening of the complexation properties of various classes of chelating molecules towards elements of interest in the fields of energy, toxicology and the environment

Acknowledgments

The authors would like to acknowledge the Cross-Disciplinary Program on Instrumentation and Detection of CEA, the French Alternative Energies and Atomic Energy Commission and the Cross-cutting basic research Program (RTA Program) of the CEA Energy Division, for their financial support.

Figures

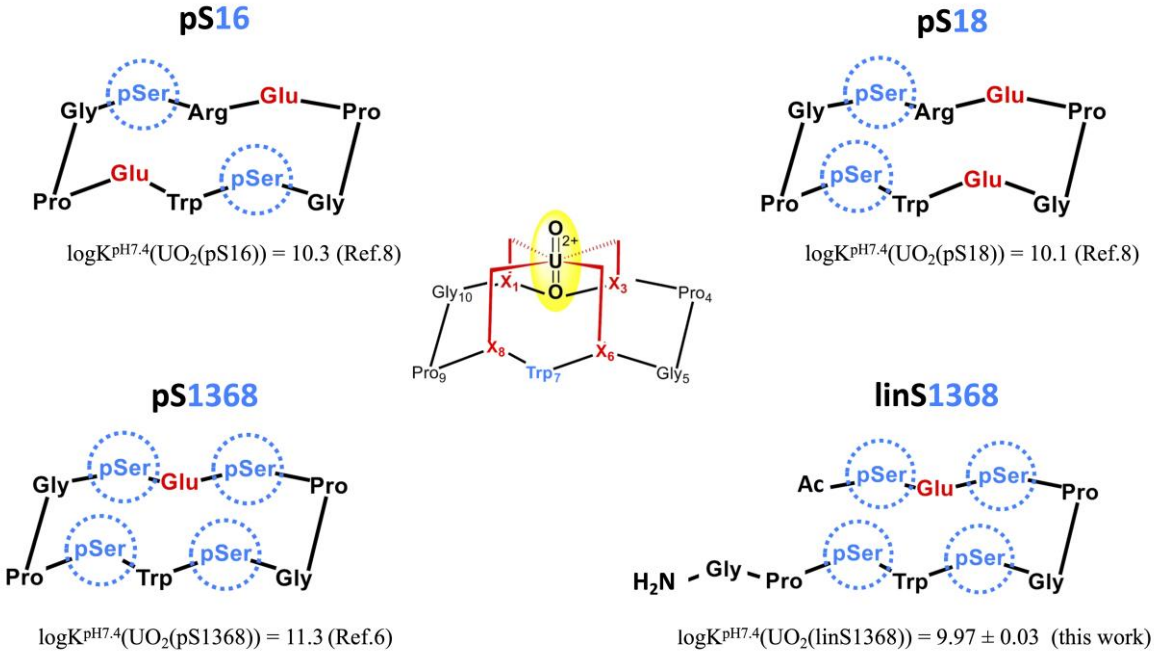

Fig.1: Multi-phosphorylated peptides considered in this work. Peptides were named according to their cyclic/linear structure and to the number and position of the pSer residues. Di-phosphorylated peptides pS18 and pS16, contain two pSer residues in trans 1,6 and cis 1,8 positions respectively. Tetra-phosphorylated pS1368 and linS1368 peptides contain four pSer residues in 1,3,6 and 8 position but have cyclic and linear structure.

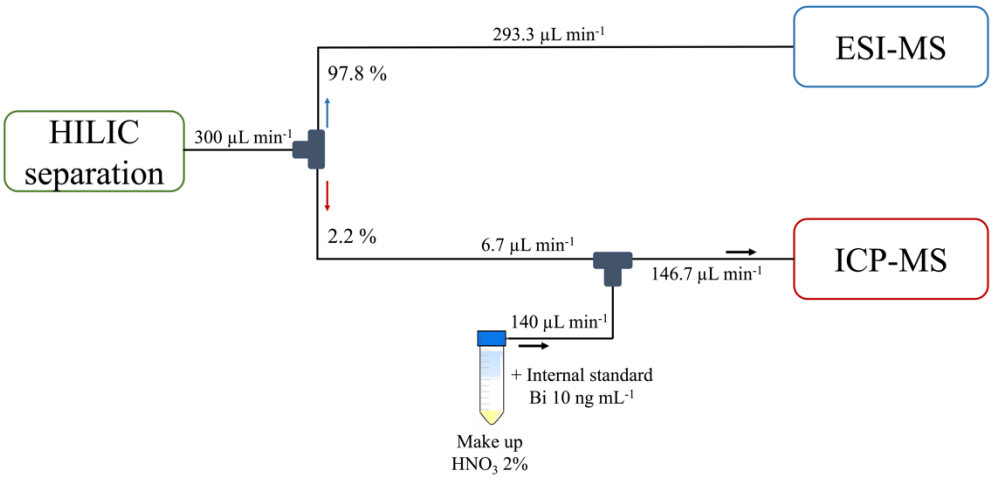

Fig.2: Schematic representation of the simultaneous coupling of HILIC to ESI-MS and ICP-MS according to [11].

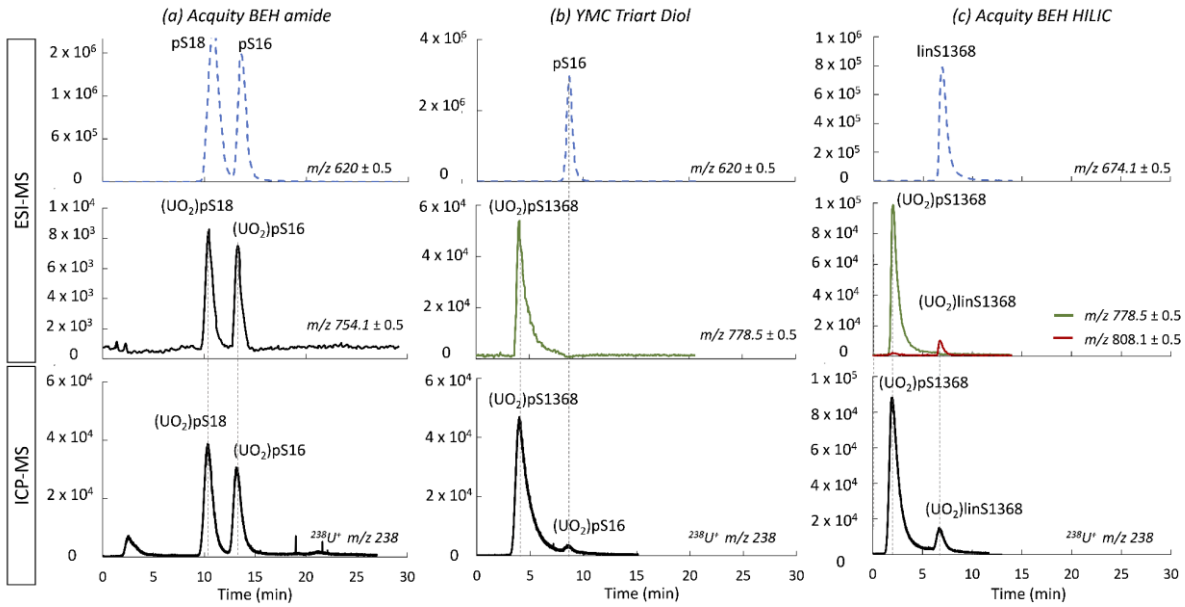

Fig.3: Chromatograms simultaneously acquired by ESI-MS using SIM mode for targeted monitoring of *m/z* ratios of free peptides and UO_2(peptide) complexes and by ICP-MS recording the ^{238}U signal with an integration time of 90 ms. (a) Sample: $2UO_2^{2+}$:10pS16:10pS18. Column: Acquity BEH amide 100 x 2.1 mm; 1.7µm. Mobile phase: 70/30 ACN/H_2O *v/v* with 20 mmol L^{-1} $NH_4CH_3CO_2$. (b) Sample: $2UO_2^{2+}$:0.5pS1368:20pS16. Column: YMC Triart Diol 100 x 2,1 mm; 1,9 µm. Mobile phase: 72/28 ACN/H_2O *v/v* with 20 mmol L^{-1} $NH_4CH_3CO_2$. (c) Sample: $2UO_2^{2+}$:0.5pS1368:3.5linS1368. Column: Acquity BEH HILIC 100 x 2,1; 1,7 µm. Mobile phase: 68/32 ACN/H_2O *v/v* with 20 mmol L^{-1} $NH_4CH_3CO_2$. In all cases, the flow rate was 300 µL min^{-1}, the elution mode isocratic and V_{inj} = 3 µL.

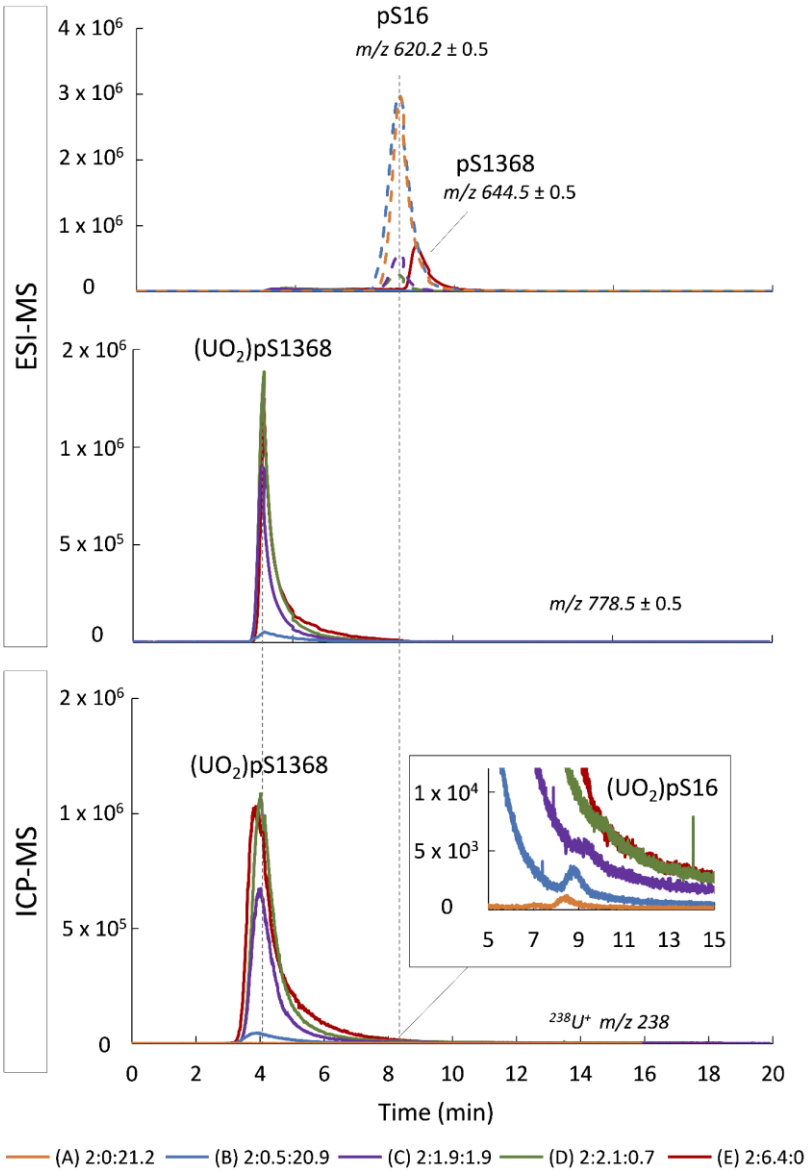

Fig.4: Chromatograms simultaneously acquired by ESI-MS using SIM mode for targeted monitoring of *m/z* ratios of free peptides and UO_2(peptide) complexes and by ICP-MS recording the ^{238}U signal with an integration time of 90 ms. Column: YMC Triart Diol 100 x 2.1 mm; 1.9 µm. Mobile phase: 72/28 ACN/H_2O v/v with 20 mmol L^{-1} $NH_4CH_3CO_2$. Flow rate was 300 µL min^{-1}, the elution mode isocratic and V_{inj} = 3 µL.

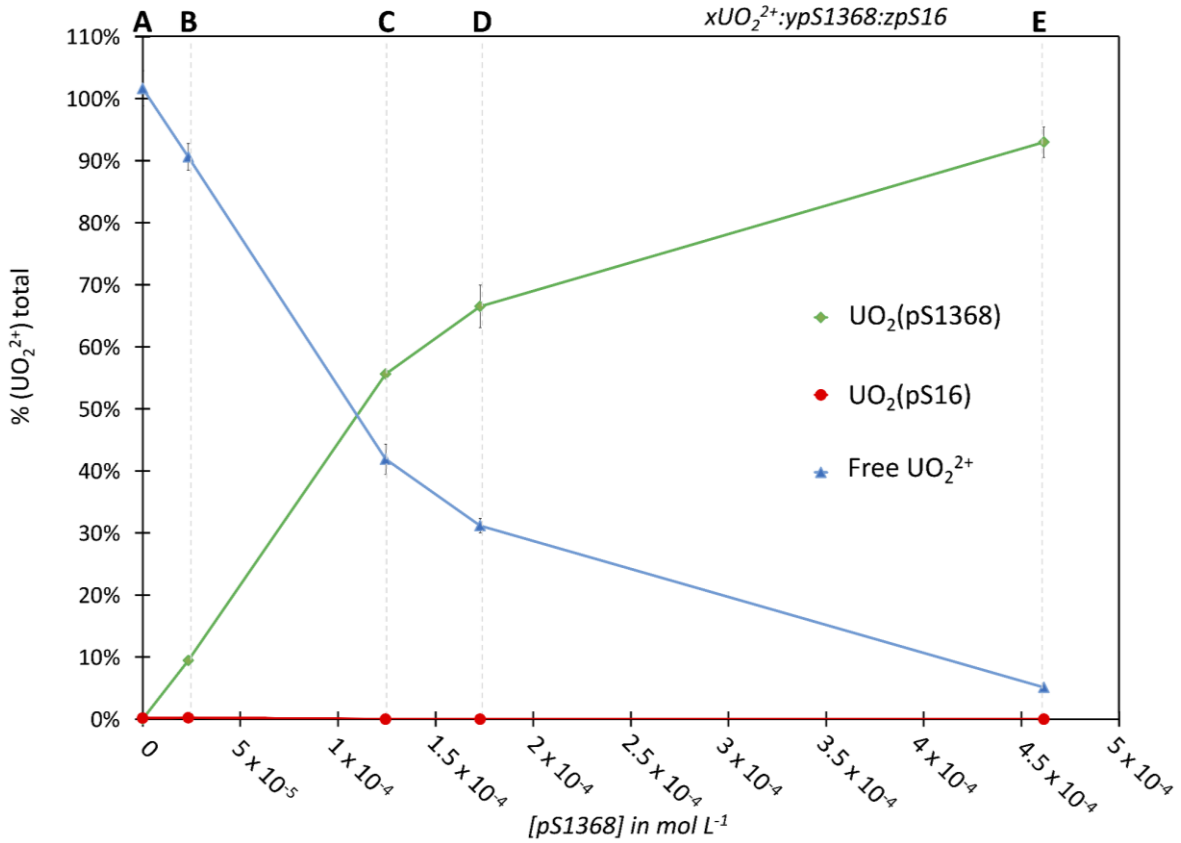

Fig.5 : Quantitative distribution of total UO_2^{2+} expressed in percentage (%) among the different complexes as a function of pS1368 concentration and xUO_2^{2+}:ypS1368:zpS16 proportions in the samples (A) 2:0:21.2, (B) 2:0.5:20.9, (C) 2:1.9:1.9, (D) 2:2.1:0.7and (E) 2:6.4:0 with average mass balance of 101.8±3%, 100.3±2%, 97.5±2%, 97.7±5%, 98.1±3%, respectively. The dots correspond to the average of the values of two replicates and the error bars represent their standard deviation.

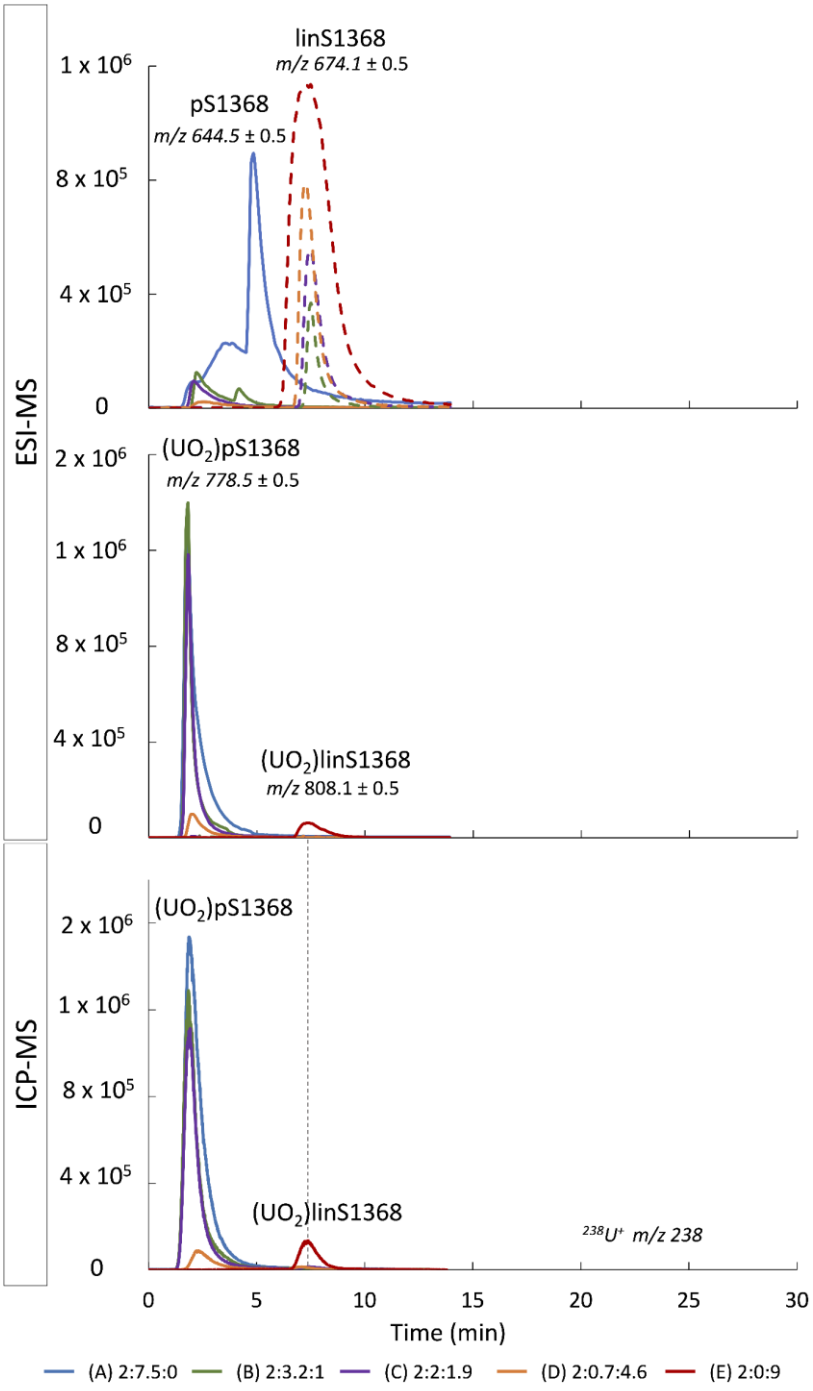

Fig.6: Chromatograms simultaneously acquired by ESI-MS using SIM mode for targeted monitoring of *m/z* ratios of free peptides and UO_2 complexes and by ICP-MS recording the ^{238}U signal with an integration time of 90 ms. Column: Acquity BEH HILIC 100 x 2,1 mm; 1,7 µm. Mobile phase: 68/32 ACN/H_2O v/v with 20 mmol L^{-1} $NH_4CH_3CO_2$. Flow rate was 300 µL min^{-1}, the elution mode isocratic and V_{inj} = 3 µL.

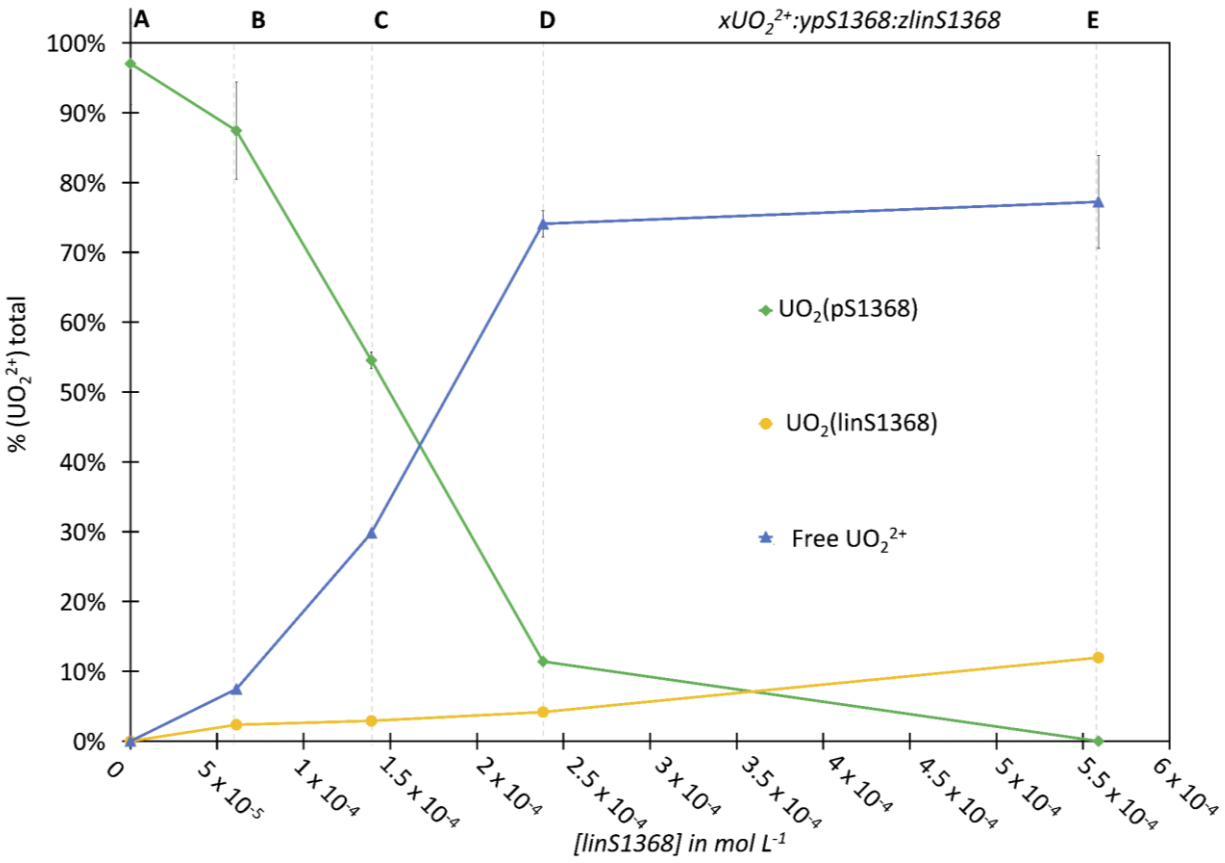

Fig.7 : Quantitative distribution of total UO_2^{2+} expressed in percentage (%) among the different complexes as a function of linS1368 concentration and the xUO_2^{2+}:ypS1368:zlinS1368 proportions in the samples (A) 2-7,5-0, (B) 2-3,2-1, (C) 2-2-1,9, (D) 2-0,7-4,6 and (E) 2-0-9 with average mass balance of 97.0±6%, 97.3±7%, 87.3±1%, 89.7±1% and 89.2±6%, respectively. The dots correspond to the average of the values of two replicates and the error bars represent their standard deviation.

Figure captions

Fig.1: Multi-phosphorylated peptides considered in this work. Peptides were named according to their cyclic/linear structure and to the number and position of the pSer residues. Di-phosphorylated peptides pS18 and pS16, contain two pSer residues in trans 1,6 and cis 1,8 positions respectively. Tetra-phosphorylated pS1368 and linS1368 peptides contain four pSer residues in 1,3,6 and 8 position but have cyclic and linear structure.

Fig.2: Schematic representation of the simultaneous coupling of HILIC to ESI-MS and ICP-MS according to [11].

Fig.3: Chromatograms simultaneously acquired by ESI-MS using SIM mode for targeted monitoring of *m/z* ratios of free peptides and UO_2(peptide) complexes and by ICP-MS recording the ^{238}U signal with an integration time of 90 ms. (a) Sample: $2UO_2^{2+}$:10pS16:10pS18. Column: Acquity BEH amide 100 x 2.1 mm; 1.7µm. Mobile phase: 70/30 ACN/H_2O *v/v* with 20 mmol L^{-1} $NH_4CH_3CO_2$. (b) Sample: $2UO_2^{2+}$:0.5pS1368:20pS16. Column: YMC Triart Diol 100 x 2,1 mm; 1,9 µm. Mobile phase: 72/28 ACN/H_2O *v/v* with 20 mmol L^{-1} $NH_4CH_3CO_2$. (c) Sample: $2UO_2^{2+}$:0.5pS1368:3.5linS1368. Column: Acquity BEH HILIC 100 x 2,1; 1,7 µm. Mobile phase: 68/32 ACN/H_2O *v/v* with 20 mmol L^{-1} $NH_4CH_3CO_2$. In all cases, the flow rate was 300 µL min^{-1}, the elution mode isocratic and V_{inj} = 3 µL.

Fig.4: Chromatograms simultaneously acquired by ESI-MS using SIM mode for targeted monitoring of *m/z* ratios of free peptides and UO_2(peptide) complexes and by ICP-MS recording the ^{238}U signal with an integration time of 90 ms. Column: YMC Triart Diol 100 x 2.1 mm; 1.9 µm. Mobile phase: 72/28 ACN/H_2O v/v with 20 mmol L^{-1} $NH_4CH_3CO_2$. Flow rate was 300 µL min^{-1}, the elution mode isocratic and V_{inj} = 3 µL.

Fig.5 : Quantitative distribution of total UO_2^{2+} expressed in percentage (%) among the different complexes as a function of pS1368 concentration and xUO_2^{2+}:ypS1368:zpS16 proportions in the samples (A) 2:0:21.2, (B) 2:0.5:20.9, (C) 2:1.9:1.9, (D) 2:2.1:0.7and (E) 2:6.4:0 with average mass

balance of 101.8±3%, 100.3±2%, 97.5±2%, 97.7±5%, 98.1±3%, respectively. The dots correspond to the average of the values of two replicates and the error bars represent their standard deviation.

Fig.6: Chromatograms simultaneously acquired by ESI-MS using SIM mode for targeted monitoring of *m/z* ratios of free peptides and UO_2 complexes and by ICP-MS recording the ^{238}U signal with an integration time of 90 ms. Column: Acquity BEH HILIC 100 x 2,1 mm; 1,7 µm. Mobile phase: 68/32 ACN/H_2O v/v with 20 mmol L^{-1} $NH_4CH_3CO_2$. Flow rate was 300 µL min^{-1}, the elution mode isocratic and V_{inj} = 3 µL.

Fig.7 : Quantitative distribution of total UO_2^{2+} expressed in percentage (%) among the different complexes as a function of linS1368 concentration and the xUO_2^{2+}:ypS1368:zlinS1368 proportions in the samples (A) 2-7,5-0, (B) 2-3,2-1, (C) 2-2-1,9, (D) 2-0,7-4,6 and (E) 2-0-9 with average mass balance of 97.0±6%, 97.3±7%, 87.3±1%, 89.7±1% and 89.2±6%, respectively. The dots correspond to the average of the values of two replicates and the error bars represent their standard deviation.

References

[1] M. Ma, R. Wang, L. Xu, M. Xu, S. Liu, Emerging health risks and underlying toxicological mechanisms of uranium contamination: Lessons from the past two decades, Environment International. 145 (2020) 106107. https://doi.org/10.1016/j.envint.2020.106107.

[2] E. Ansoborlo, O. Prat, P. Moisy, C. Den Auwer, P. Guilbaud, M. Carriere, B. Gouget, J. Duffield, D. Doizi, T. Vercouter, C. Moulin, V. Moulin, Actinide speciation in relation to biological processes, Biochimie. 88 (2006) 1605–1618. https://doi.org/10.1016/j.biochi.2006.06.011.

[3] C. Basset, O. Averseng, P.-J. Ferron, N. Richaud, A. Hagège, O. Pible, C. Vidaud, Revision of the Biodistribution of Uranyl in Serum: Is Fetuin-A the Major Protein Target?, Chem. Res. Toxicol. 26 (2013) 645–653. https://doi.org/10.1021/tx400048u.

[4] L. Qi, C. Basset, O. Averseng, E. Quéméneur, A. Hagège, C. Vidaud, Characterization of UO_2^{2+} binding to osteopontin, a highly phosphorylated protein: insights into potential mechanisms of uranyl accumulation in bones, Metallomics. 6 (2014) 166–176. https://doi.org/10.1039/C3MT00269A.

[5] A. Garai, P. Delangle, Recent advances in uranyl binding in proteins thanks to biomimetic peptides, Journal of Inorganic Biochemistry. 203 (2020) 110936. https://doi.org/10.1016/j.jinorgbio.2019.110936.

[6] F.A. Laporte, C. Lebrun, C. Vidaud, P. Delangle, Phosphate-Rich Biomimetic Peptides Shed Light on High-Affinity Hyperphosphorylated Uranyl Binding Sites in Phosphoproteins, Chemistry – A European Journal. (2019). https://doi.org/10.1002/chem.201900646.

[7] C. Lebrun, M. Starck, V. Gathu, Y. Chenavier, P. Delangle, Engineering Short Peptide Sequences for Uranyl Binding, Chem. Eur. J. 20 (2014) 16566–16573. https://doi.org/10.1002/chem.201404546.

[8] M. Starck, N. Sisommay, F.A. Laporte, S. Oros, C. Lebrun, P. Delangle, Preorganized Peptide Scaffolds as Mimics of Phosphorylated Proteins Binding Sites with a High Affinity for Uranyl, Inorg. Chem. 54 (2015) 11557–11562. https://doi.org/10.1021/acs.inorgchem.5b02249.

[9] M. Starck, F.A. Laporte, S. Oros, N. Sisommay, V. Gathu, P.L. Solari, G. Creff, J. Roques, C. Den Auwer, C. Lebrun, P. Delangle, Cyclic Phosphopeptides to Rationalize the Role of Phosphoamino Acids in Uranyl Binding to Biological Targets, Chem. Eur. J. 23 (2017) 5281–5290. https://doi.org/10.1002/chem.201605481.

[10] F. Laporte, Y. Chenavier, A. Botz, C. Gateau, C. Lebrun, S. Hostachy, C. Vidaud, P. Delangle, A Simple Fluorescence Affinity Assay to Decipher Uranyl-Binding to Native Proteins, Angew Chem Int Ed. 61 (2022). https://doi.org/10.1002/anie.202203198.

[11] E. Blanchard, A. Nonell, F. Chartier, A. Rincel, C. Bresson, Evaluation of superficially and fully porous particles for HILIC separation of lanthanide–polyaminocarboxylic species and simultaneous coupling to ESIMS and ICPMS, RSC Adv. 8 (2018) 24760–24772. https://doi.org/10.1039/C8RA02961J.

[12] H. Peng, B. Hu, Q. Liu, Z. Yang, X. Lu, R. Huang, X.-F. Li, M.J. Zuidhof, X.C. Le, Liquid chromatography combined with atomic and molecular mass spectrometry for speciation of arsenic in chicken liver, Journal of Chromatography A. 1370 (2014) 40–49. https://doi.org/10.1016/j.chroma.2014.10.012.

[13] A. Hagège, T.N.S. Huynh, M. Hébrant, Separative techniques for metalloproteomics require balance between separation and perturbation, TrAC Trends in Analytical Chemistry. 64 (2015) 64–74.

https://doi.org/10.1016/j.trac.2014.08.013.

[14] J. Köster, R. Shi, N. von Wirén, G. Weber, Evaluation of different column types for the hydrophilic interaction chromatographic separation of iron-citrate and copper-histidine species from plants, Journal of Chromatography A. 1218 (2011) 4934–4943. https://doi.org/10.1016/j.chroma.2011.03.036.

[15] E. Paredes, E. Avazeri, V. Malard, C. Vidaud, P.E. Reiller, R. Ortega, A. Nonell, H. Isnard, F. Chartier, C. Bresson, Evidence of isotopic fractionation of natural uranium in cultured human cells, Proc Natl Acad Sci USA. 113 (2016) 14007–14012. https://doi.org/10.1073/pnas.1610885113.

[16] A. Leclercq, A. Nonell, J.L. Todolí Torró, C. Bresson, L. Vio, T. Vercouter, F. Chartier, Introduction of organic/hydro-organic matrices in inductively coupled plasma optical emission spectrometry and mass spectrometry: A tutorial review. Part I. Theoretical considerations, Analytica Chimica Acta. 885 (2015) 33–56. https://doi.org/10.1016/j.aca.2015.03.049.

[17] A. Leclercq, A. Nonell, J.L. Todolí Torró, C. Bresson, L. Vio, T. Vercouter, F. Chartier, Introduction of organic/hydro-organic matrices in inductively coupled plasma optical emission spectrometry and mass spectrometry: A tutorial review. Part II. Practical considerations, Analytica Chimica Acta. 885 (2015) 57–91. https://doi.org/10.1016/j.aca.2015.04.039.

[18] M. Sutton, S.R. Burastero, Uranium(VI) Solubility and Speciation in Simulated Elemental Human Biological Fluids, Chem. Res. Toxicol. 17 (2004) 1468–1480. https://doi.org/10.1021/tx049878k.

[19] A. Younes, G. Creff, M.R. Beccia, P. Moisy, J. Roques, J. Aupiais, C. Hennig, P.L. Solari, C. Den Auwer, C. Vidaud, Is hydroxypyridonate 3,4,3-LI(1,2-HOPO) a good competitor of fetuin for uranyl metabolism?, Metallomics. 11 (2019) 496–507. https://doi.org/10.1039/C8MT00272J.

[20] C. Vidaud, M. Robert, E. Paredes, R. Ortega, E. Avazeri, L. Jing, J.-M. Guigonis, C. Bresson, V. Malard, Deciphering the uranium target proteins in human dopaminergic SH-SY5Y cells, Arch Toxicol. 93 (2019) 2141–2154. https://doi.org/10.1007/s00204-019-02497-4.

[21] Y. Eb-Levadoux, S. Frelon, O. Simon, C. Arnaudguilhem, R. Lobinski, S. Mounicou, In vivo identification of potential uranium protein targets in zebrafish ovaries after chronic waterborne exposure, Metallomics. 9 (2017) 525–534. https://doi.org/10.1039/C6MT00291A.

[22] S. Frelon, O. Simon, Y. Eb-Levadoux, S. Mounicou, Screening of potential uranium protein targets in fish ovaries after chronic waterborne exposure: Differences and similarities between roach and zebrafish, Journal of Environmental Radioactivity. 222 (2020) 106365. https://doi.org/10.1016/j.jenvrad.2020.106365.

[23] Ł. Szyrwiel, V. Liauchuk, L. Chavatte, R. Lobinski, In vitro induction and proteomics characterisation of a uranyl–protein interaction network in bovine serum, Metallomics. 7 (2015) 1604–1611. https://doi.org/10.1039/C5MT00207A.

[24] A. Dedieu, F. Bérenguer, C. Basset, O. Prat, E. Quéméneur, O. Pible, C. Vidaud, Identification of uranyl binding proteins from human kidney-2 cell extracts by immobilized uranyl affinity chromatography and mass spectrometry, Journal of Chromatography A. 1216 (2009) 5365–5376. https://doi.org/10.1016/j.chroma.2009.05.023.

[25] L. Abou Zeid, A. Pell, T. Tytus, P. Delangle, C. Bresson, Separation of multiphosphorylated cyclopeptides and their positional isomers by hydrophilic interaction liquid chromatography (HILIC) coupled to electrospray ionization mass spectrometry (ESI-MS), Journal of Chromatography B. 1177 (2021) 122792. https://doi.org/10.1016/j.jchromb.2021.122792.

[26] M. Birka, K.S. Wentker, E. Lusmöller, B. Arheilger, C.A. Wehe, M. Sperling, R. Stadler, U. Karst, Diagnosis of Nephrogenic Systemic Fibrosis by means of Elemental Bioimaging and Speciation Analysis, Anal. Chem. 87 (2015) 3321–3328. https://doi.org/10.1021/ac504488k.

[27] G. Weber, N. von Wirén, H. Hayen, Hydrophilic interaction chromatography of small metal species in plants using sulfobetaine- and phosphorylcholine-type zwitterionic stationary phases, Journal of Separation Science. 31 (2008) 1615–1622. https://doi.org/10.1002/jssc.200800060.

[28] J. Vanhorn, H. Huang, Uranium(VI) bio-coordination chemistry from biochemical, solution and protein structural data, Coordination Chemistry Reviews. 250 (2006) 765–775. https://doi.org/10.1016/j.ccr.2005.09.010.

[29] S. Safi, G. Creff, A. Jeanson, L. Qi, C. Basset, J. Roques, P.L. Solari, E. Simoni, C. Vidaud, C. Den Auwer, Osteopontin: A Uranium Phosphorylated Binding-Site Characterization, Chemistry - A European Journal. 19 (2013) 11261–11269. https://doi.org/10.1002/chem.201300989.

[30] R. Pardoux, S. Sauge-Merle, D. Lemaire, P. Delangle, L. Guilloreau, J.-M. Adriano, C. Berthomieu, Modulating Uranium Binding Affinity in Engineered Calmodulin EF-Hand Peptides: Effect of Phosphorylation, PLoS ONE. 7 (2012) e41922. https://doi.org/10.1371/journal.pone.0041922.

[31] S. Sauge-Merle, F. Brulfert, R. Pardoux, P.L. Solari, D. Lemaire, S. Safi, P. Guilbaud, E. Simoni, M.L. Merroun, C. Berthomieu, Structural Analysis of Uranyl Complexation by the EF-Hand Motif of Calmodulin: Effect of Phosphorylation, Chem. Eur. J. 23 (2017) 15505–15517. https://doi.org/10.1002/chem.201703484.

[32] H. Zänker, K. Heine, S. Weiss, V. Brendler, R. Husar, G. Bernhard, K. Gloe, T. Henle, A. Barkleit, Strong Uranium(VI) Binding onto Bovine Milk Proteins, Selected Protein Sequences, and Model Peptides, Inorganic Chemistry. 58 (2019) 4173–4189. https://doi.org/10.1021/acs.inorgchem.8b03231.

[33] F. Laporte, Compréhension des mécanismes de complexation de l'uranyle par les molécules du vivant: élaboration de peptides biomimétiques chélatants pour la détoxification, PhD Thesis, Grenoble Alpes, 2017.